Highly sensitive detection of bacteria (*E. Coli*) endotoxin using novel PANI-benzimidazole-Ag nanocomposite by DMMB dye displacement assay

To cite this article: Tadele Ageru Alemu *et al* 2023 *Mater. Res. Express* **10** 075302

Materials Research Express

PAPER

Highly sensitive detection of bacteria (*E. Coli*) endotoxin using novel PANI-benzimidazole-Ag nanocomposite by DMMB dye displacement assay

Tadele Ageru Alemu[1], **Delele Worku Ayele**[2], **J Shahitha Parveen**[3], **Ababay Ketema Worku**[4], **Minbale Admas Teshager**[2], **Praveen C Ramamurthy**[5] and **Dhakshnamoorthy Mani**[1,*]

[1] Faculty of Materials Science and Engineering, Jimma Institute of Technology, Jimma University, Jimma, PO Box. 378, Ethiopia
[2] Department of Chemistry, College of Science, Bahir Dar University, Bahir Dar, PO Box. 79, Ethiopia
[3] Department of Polymer Engineering. B.S. Abdur Rahman Crescent Institute of Science & Technology, Chennai, Postal Code. 600048, India
[4] Bahir Dar Energy Center, Bahir Dar Institute of Technology, Bahir Dar University, Bahir Dar PO Box 26, Ethiopia
[5] Department of Materials Engineering, Indian Institution of Science (IISC), Bangalore, Postal Code. 560012, India
[*] Author to whom any correspondence should be addressed.

E-mail: delelewww@gmail.com **and** dhakshnamoorthy.mani@ju.edu.et

Keywords: PANI-benzimidazole-Ag nanocomposite endotoxin, (E. Coli) detection, DMMB dye displacement hitchhiking confocal, fluorescence imaging microscopy

OPEN ACCESS

RECEIVED
30 March 2023

REVISED
19 June 2023

ACCEPTED FOR PUBLICATION
27 June 2023

PUBLISHED
7 July 2023

Abstract

In the present study, a new biochemical biosensor material of conductive Silver (Ag) reinforced polyaniline (PANI)-Benzimidazole copolymer nanocomposite was fabricated via *in situ* chemical oxidative polymerization method for the detection of endotoxin. The fabricated PANI-Benz-Ag nanocomposite was characterized by FTIR, XRD, UV–visible spectrometer, DSC, TGA, Zeta-potential, SEM, TEM, and Confocal fluorescence imaging microscopy. The measured particle size, zeta-potential, and conductivity of the PANI-Benz-Ag nanocomposite were 4.942 nm, −10.4 mV, and 73.7 μS cm^{-1} respectively. The crystallite size of Ag nanoparticles was around 67 nm calculated by XRD analysis and TGA analysis was carried out to determine weight loss and thermal stabilities of PANI-Benz and PANI-Benz-Ag nanocomposite. The endotoxin *(E. coli)* bacteria detection ability of the synthesized PANI-Benz-Ag nanocomposite-based biochemical biosensor using DMMB dye displacement assay through the hitchhiking method by confocal fluorescence microscopy was found to be simple and effective. Endotoxin *(E. coli)* can form a stable interaction with other bioactive molecules and thus it binds readily with Ag-doped PANI-Benzimidazole nanocomposite. Further, the DMMB dye displacement assay method is more accurate and sensitive than the other existing methods for the detection of endotoxin.

1. Introduction

Endotoxin bacterial contaminated (adulterated and putrefied) foods have a detrimental effect on human health which is a serious problem throughout the world [1–4]. Endotoxins are lipopolysaccharides (LPS) found in the outer membrane of the cell wall of Gram-negative bacteria which can induce inflammation and fever as an immune response in higher organisms [5–8]. Contamination of foods due to Endotoxins bacteria occurred either at any point during its processing or production at home or shops when not properly handled. Endotoxins specifically *Escherichia Coli* (*E. coli*) bacteria come in contact with the body through poised foods, it stimulates antigenic responses to gram-negative infections since the presence of lipid A (active part) of LPS which is the primary toxic component and responsible for the toxic behavior [9–11].

Endotoxin *(E. coli)* Bacteria infections occurred and harmed people due to the contamination of plant foods (fresh fruits, lettuce, spinach, tomato, etc) [12]. The prevalence of *E. coli* Bacteria has been checked in a variety of extremely small extent processed vegetables and fruits [12]. Fruit Juices such as Mango Juice, Avocado Juice, etc

are highly perishable and can serve as an ideal medium for the growth and multiplication of various pathogenic microorganisms like Endotoxin (*E. coli*) and other bacterial species. The endotoxin-contaminated fruit juices may cause typhoid fever, food poisoning, gastroenteritis, enteric fever, diarrheal disease, and/or human foodborne diseases [WHO, 7 February 2018, [13–17]]. According to the world health organization (WHO) statement, the *E. coli* bacteria-type outbreak caused a loss of US$1.3 billion to Germany's farmers and industries and required payments of US$236 million in emergency aid to 22 European Union member state in 2011 [18]. This clearly indicates that pathogenic *E. coli* foodborne due to contamination of fruit Juice and its outbreak is still a significant human illness throughout the world [18]. Besides, different outbreaks of infectious diseases due to contamination of fruit Juices with pathogenic microorganisms like Endotoxin (*E. coli*) bacterial species have brought in high morbidity and mortality [19–21]. According to a 2017 WHO report, the annual global burden of foodborne diseases was about 600 million of which 420,000 people die, including 125,000 children under the age of 5 years [22–25].

According to human health and economic consequences of Endotoxin bacteria, different research works have been conducted on the conventional methods for the detection of Endotoxins [5, 26]. The Rabbit pyrogen test was the 1st method and was replaced by the Limulus Amoebocyte test which is the most popular detection technique for Endotoxins and electrochemical biosensors using biomolecules as well as artificial materials [27, 28]. The recent approaches focus on the Rabbit pyrogen test and the Limulus Amoebocyte test for the detection of Endotoxin in various biological products. Moreover, different scholars reported and reviewed the current trends in Endotoxin detection and analysis of Endotoxin-Protein interactions [29]. Cao *et al* investigated the gold nanoparticle-reinforced molybdenum disulfide-polyacrylic acid nanocomposite [30]. Low endotoxin recovery and its impact on endotoxin detection and confocal fluorescent imaging method for quantification of protein by collecting data on a confocal microscope and quantitating the relative levels of a molecule by measuring mean fluorescent intensity across a region of interest (ROI) were reported [30, 31]. However, highly emphasized, crucial, and very considerable thematic area but to the best of our knowledge, no studies have been reported on sensors for Endotoxins (e.g., *E. coli* bacteria) for the detection of food poisoning especially poisoned mango juice.

The other existing techniques depend on metal oxide semiconductor (MOS) based sensors but they have their own limitations/drawbacks such as high operating temperatures that cause high-power consumption which means cannot be handheld materials as well as need very skilled power while the Limulus Amoebocyte Lysate (LAL) and Rapid Pyrogen Test have been conducted for only animal blood samples and also these are not rapid, accurate and sensitive methods for pathogenic bacteria in human blood compared to the recent method [29, 32, 33]. In this work, we have fabricated a novel silver nanoparticle reinforced polyaniline—Benzimidazole (PANI-Benz-Ag) nanocomposite-based electrochemical biosensor for the detection of *E. coli* bacteria in poisoned Mango juice using 1, 9-Dimethyl-methylene blue zinc chloride Assay (DMMB) method by confocal fluorescence microscopy. The polyaniline-Benzimidazole copolymer was prepared by *in situ* chemical oxidative polymerization method. Silver (Ag) nanoparticles were doped by reacting with $AgNO_3$ with the copolymer to prepare a PANI-Benz-Ag nanocomposite (bioactive) sensor. This biochemical sensor can be utilized at room temperature for the detection of endotoxin. The principle of detection is based on measuring the physical contacts via a biological binding process dependent on intensity changes on the surface of the electrochemical biosensor.

2. Experimental methods

2.1. Materials

Aniline (99.9%, Sigma-Aldrich), Benzimidazole (>98%, Biocrick), Silver nitrate (99.8%, Sigma-Aldrich), N-Methyl-2-Pyrrolidone (98.5%), p-Toluene sulfonic acid (98%), Acetone (98%), Diethyl ether (98%), Azobisisobutyronitrile (AIBN, 99.5%), Ethanol (99%), 1, 9-Dimethyl-methylene blue zinc chloride (99.5%, Sigma-Aldrich) were purchased from M/s. Spectrochem, India. Endotoxin bacteria, TG1 (*E. coli* strain standard usage for 0.5 M purpose cultured at 37 °C from the Department of Microbiology and Cell Biology, Indian Institute of Science, India.

2.2. Preparation of polyaniline-benzimidazole-ag nanocomposite

At first, polyaniline was synthesized by *in situ* chemical oxidative polymerization. Aniline (5 g) was added with 1 g of p-Toluene sulfonic acid (an acidic dopant to control stereo-regularity as a stabilizer) in a 500 ml flask. Then, 15 ml of N-methyl-2pyrrolidone (NMP) solvent was added to the mixture which was kept on the ice bath (below 5 °C) under vigorous stirring conditions for 10 min The 5 g of Azobis-isobutyronitrile (AIBN, free-radical initiator) was added to the reaction mixture and stirred for 24 h at 5 °C to complete the oxidative polymerization reaction. The dark green solution was obtained and then 60 ml of acetone, 60 ml of diethyl ether,

and 20 ml of ethanol were added to the solution. The solution was filtered and the precipitate (PANI) was washed with de-ionized water until the filtrate becomes colorless. The oligomeric impurities have been removed from the precipitate by washing with methanol and acetone. The PANI precipitate was dried in a vacuum oven at 60 °C for 12 h and ground into a powder [34].

The polyaniline-benzimidazole (PANI-Benz) copolymer was prepared by mixing Aniline (3 g) and Benzimidazole (2 g) after following the above procedures. A similar method was followed for the synthesis of PANI-Ag (5%) and PANI-Benz-Ag (5%) nanocomposite by adding 0.25 g of silver nitrate, $AgNO_3$ with PANI-Benzimidazole reaction mixture using *in situ* chemical polymerization method [35].

2.3. Characterization

Fourier transform infrared (FTIR) spectroscopic results were obtained from an FTIR spectrometer (spectrum one, Perkin Elmer, Waltham, MA, USA) with an ATR transmission mode in the wavelength range of 400–4000 cm^{-1}. The x-ray diffraction (XRD) study was carried out with Cu Kα radiation ($\lambda = 0.1541$ nm), an accelerating potential of 40 kV, and a current of 30 mA at a scanning rate of 0.5° min^{-1} on an x-ray diffractometer (Rigaku MultiFlex ZD3609N). The Surface morphology of PANI-Benz-Ag nanocomposite was investigated by Field Emission Scanning electron microscope (FESEM, Carl Zeiss Ultra 55 and JSM-IT300) at an accelerating voltage of 10 kV with energy and angle selective backscattered electron (EsB) detector and Transmission electron microscopy (TEM) (Model; JSM Tecnai F_{20}). The absorbance of each sample solution was studied by UV-Vis spectrophotometer (model V-750 UV-Visible spectrophotometer) in a wavelength range of 200–800 nm. The thermal decomposition of samples was determined by a Thermogravimetric analyzer, TGA (Model: STA409PC Netzsch, Germany). The endothermic and exothermic properties were analyzed by Differential scanning calorimetric, DSC (model: DSC-822^e, Mettler, Toledo, Germany) with liquid Nitrogen, −150 °C to 700 °C and heat flow sensitivity of 0.04 mW and 0.1 °C accuracy. The size distributions and zeta potentials of the samples were determined by Zetasizer, Dynamic light scattering (Zetasizer Ver.7.13. MAL 1031019). The hitchhiking and quenching mechanisms between the synthesized nanocomposite electrochemical biosensor and endotoxin bacteria (1, 9-dimethyl methylene zinc chloride blue displacement assay) were studied by Confocal Fluorescence Microscopy (Confocal Leica TCS SP8, Hyvolution).

3. Results and discussion

Figure 1(a) shows the FTIR spectrum of PANI, PANI-Benz, and PANI-Benz-Ag nanocomposite. The absorption peaks at 2917 cm^{-1} and 1464 cm^{-1} are attributed to N-H stretching of the quinoid and C=C stretching of the benzenoid rings present in PANI respectively [36]. Absorption peaks at 3498 cm^{-1} and 1605 cm^{-1} correspond to N-H stretching vibration of the amine and the C-H stretching band of cyclic alkene. The characteristic peaks at 1592 cm^{-1} and 873 cm^{-1} are assigned to asymmetric C-H stretching and plane C-H bending vibrations of benzenoid rings respectively [37, 38]. A sharp peak at 955 cm^{-1} corresponds to the C=C bending vibration of benzimidazole [39].

The XRD pattern of PANI, PANI-Benz, and PANI-Benz-Ag nanocomposite is shown in figure 1(b). The prominent diffraction peaks at 37.8, 42.5, 63.7, 76.8, and 80.1 can be assigned to the plane of Ag crystals (111), (200), (220), (311), and (222) respectively. It confirms that the formed Ag nanoparticles are face-centered, cubic, and crystalline in nature (JCPDS 74–2251)[36]. The crystallite size of Ag nanoparticles was calculated using Bragg reflection by the Debye–Scherrer equation ($D = 0.9\lambda/\beta\cos\theta$). The average crystallite size of the PANI-Benz-Ag nanocomposite was 67 nm [36, 40].

Figure 2(a) shows the UV-Visible absorption spectrum of PANI and PANI-Benz-Ag nanocomposite. The absorption band at 365 nm and 655 nm correspond to π-π^* transition of the benzenoid ring and π-polaron transition (due to the charge transfer between the benzenoid and quinoid units) respectively [36, 41].

Differential scanning calorimetric analysis of PANI and PANI-Benz-Ag nanocomposite are shown in figure 2(b). Based on the DSC curves, PANI has only below baseline condition which indicates amorphousness ((E) Integral = −2609.20 mJ, normalized = −99.97 J g^{-1}, onset = 51.99 °C, peak at 102.97 °C and end set=148.64 °C). In PANI-Benz-Ag nanocomposite, there are two conditions; endothermic condition ((C) Integral = −47.74 mJ, normalized = −3.91 J g^{-1}, onset = 102.92 °C, peak at 103.55 °C and end set = 105.14 °C)) and exothermic condition. The PANI-Benz-Ag nanocomposite was unstable below baseline due to absorption of energy (endothermic) and there might be a rearrangement of particles by releasing heat (exothermic) and hence becoming more stable.

Figure 2(c) shows the thermogravimetric analysis curve of PANI-Benz and PANI-Benz-Ag nanocomposites. It was observed that there was a weight loss of around 7.3% and 0.82% at 98 °C for PANI-Benz and PANI-Benz-Ag nanocomposite respectively. The weight loss may be due to the evaporation of water molecules (moisture) present in the specimen. The major weight loss was observed at 247 °C which may be due to the degradation of

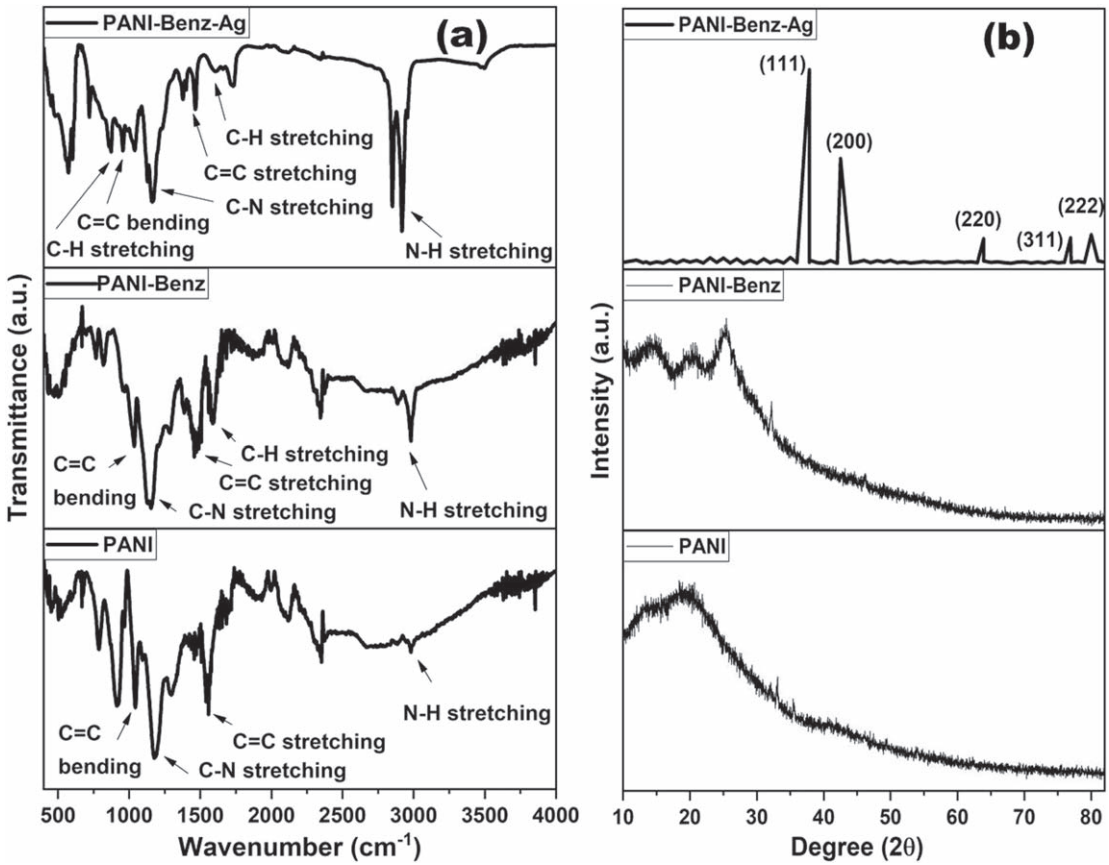

Figure 1. (a) FTIR spectra and (b) XRD pattern of PANI, PANI-Benz, and PANI-Benz-Ag nanocomposite.

PANI and evaporation of gas molecules such as H_2, etc It is clearly shown that there was a higher weight loss observed in PANI-Benz than PANI-Benz-Ag nanocomposite. The PANI-Benz-Ag nanocomposite has higher thermal stability below 100 °C and it can be used at room temperature effectively.

The size distribution reports for PANI, PANI-Benz, PANI-Ag, and PANI-Benz-Ag nanocomposite are shown in figure 3. The size distribution values are given in table 1. In principle, the size of a single unit of the nanomaterial is between 1 nm − 100 nm (at least one dimension) [42]. As per the standard BS-ISO 22412:2017, the size distribution of PANI (figure 3(a)) particles indicates an inconsistency in particle size, shape, and mass due to broad and wide peaks. Figure 3(b) PANI-Benz shows a narrow and sharp peak which indicates improved consistency in particle size, shape, and mass. The PANI-Ag nanocomposite (figure 3(c)) shows a single narrow peak but not is sharp compared to PANI and PANI-Benz peaks. This indicates that better consistency in particle size, shape, and mass for PANI-Ag nanocomposite than PANI as well as PANI-Benz. Figure 3(d) shows a narrow and sharp peak and a particle size (d) of 4.942 nm. This indicates that the PANI-Benz-Ag nanocomposite has excellent consistency in particle size, shape, and mass of the particles.

As illustrated in figures 3(a)–(d) and table 1, the particle size of PANI-Benz-Ag ($z_{ave} = 1.863$ nm) < PANI-Ag ($z_{ave} = 139.1$ nm) < PANI-Benz ($z_{ave} = 227.1$ nm) < PANI ($z_{ave} = 314.2$ nm). Thus, the smallest particle size of the PANI-Benz-Ag nanocomposite made it an excellent biochemical sensor for the detection of Endotoxin (*E. coli*) bacterial species. This is due to the smallest particle size of the PANI-Benz-Ag nanocomposite which provides effective porosity, the smallest surface area, excellent mechanical properties, thermal stability, enhanced electrical conductivity, semi-crystallinity, favorable morphology, and particle arrangements leading to excellent detection performance.

Figures 4(a)–(d) show the plots of apparent zeta potential versus total counts of PANI, PANI-Benz, PANI-Ag, and PANI-Benz-Ag nanocomposite respectively [43]. The zeta potential values are listed in table 2. It is observed that there is an increase in both zeta potential and conductivity in the order of PANI, PANI-Benz, PANI-Ag, and PANI-Benz-Ag nanocomposite. This shows that Ag nanoparticles incorporated PANI-Benz copolymer has excellent conductivity and stability. The negative potential indicates the net charge of the scattering materials to the negative slipping plane. As indicated in figure 4 and table 2, both the zeta potential and conductivity are increasing from PANI (−2.39 mV & 5.1 μS cm^{-1}), PANI-Benz (−5.47 mV & 5.2 μS cm^{-1}), PANI-Ag (−7.28 mV, & 8.52 μS cm^{-1}) to PANI-Benz-Ag (−10.4 mV, & 73.7 μS cm^{-1}) respectively. The

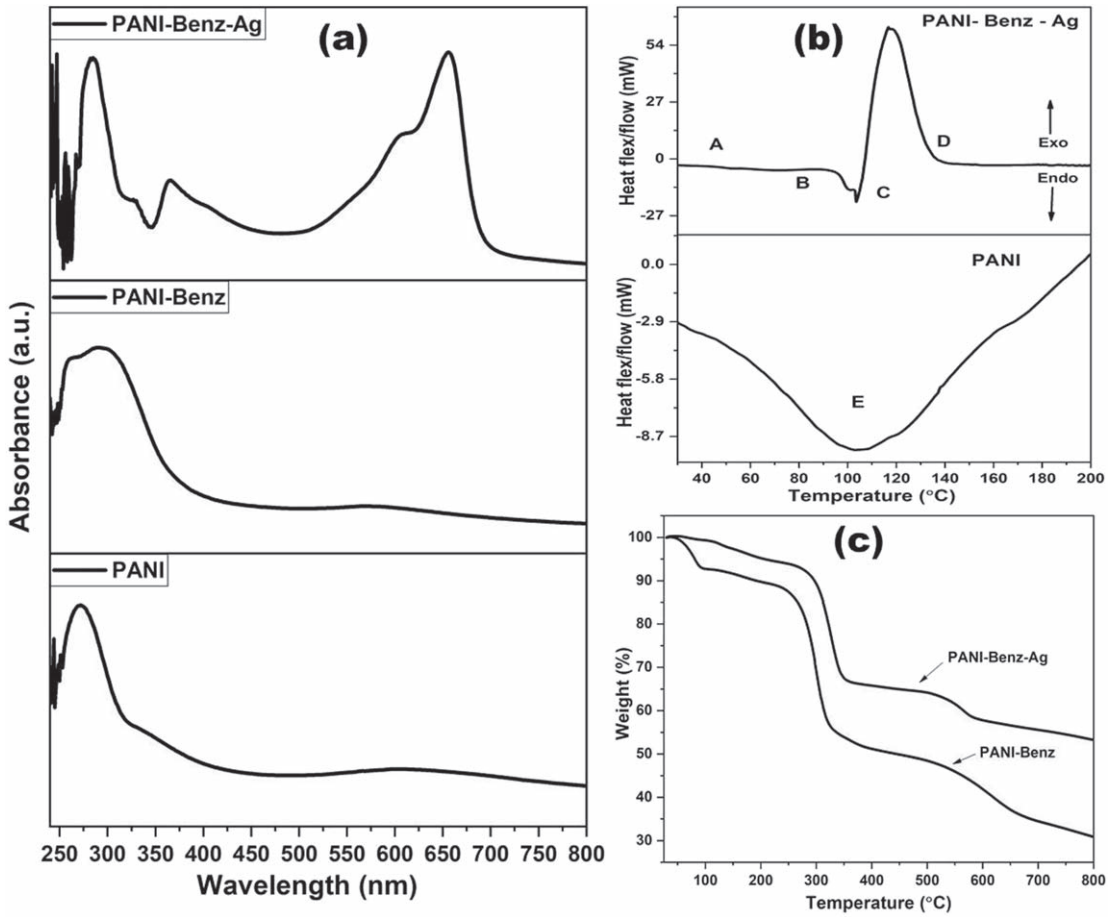

Figure 2. (a) UV-Visible absorption spectra, (b) Differential scanning calorimetric curve, and (c) Thermogravimetric analysis of PANI, PANI-Benz, and PANI-Benz-Ag nanocomposite.

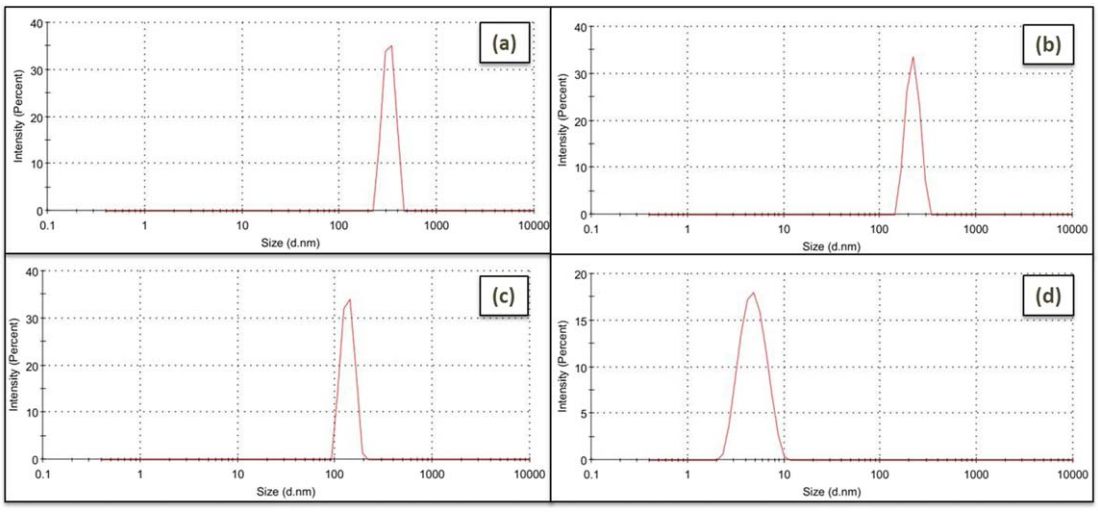

Figure 3. Size distribution reports of (a) PANI, (b) PANI-Benz copolymer, (c) PANI-Ag nanocomposite, and (d) PANI-Benz-Ag nanocomposite.

increase in zeta potential indicates the stability of the material and the negative symbol shows the net charge of the scattering material up to the negative slipping plane. However, the electrical potential at the slipping plane for PANI-Benz-Ag (−10.4 mV) is higher than PANI (−2.39 mV), PANI-Benz (−5.47 mV), PANI-Ag (−7.28 mV). In the case of PANI, PANI-Benz, and PANI-Ag, there might be more aggregation of particles and impurities than PANI-Benz-Ag nanocomposite. The zeta potential of PANI-Benz-Ag nanocomposite is higher

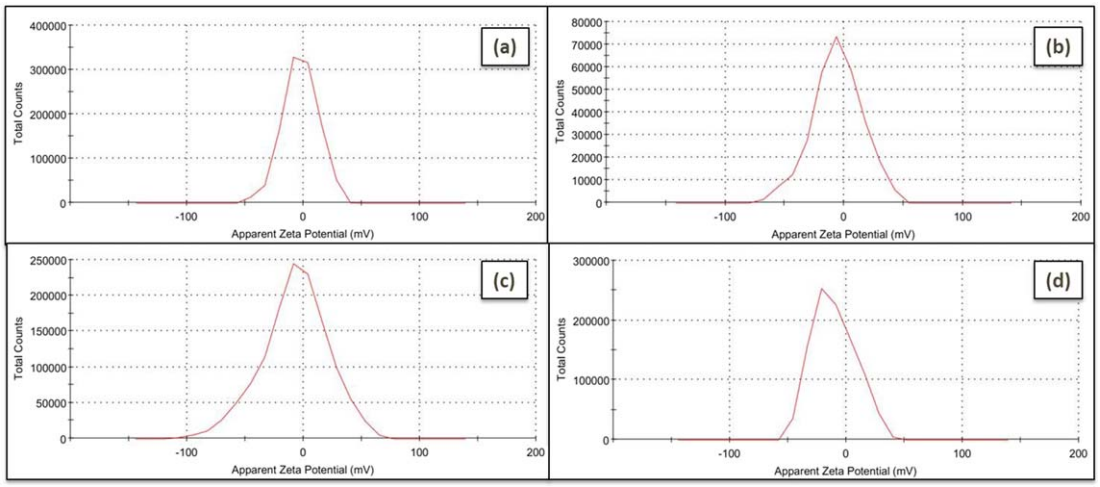

Figure 4. Zeta potential distribution reports of (a) PANI, (b) PANI-Benz copolymer, (c) PANI-Ag nanocomposite, and (d) PANI-Benz-Ag nanocomposite.

Table 1. The size distribution values of PANI, PANI-Benz, PANI-Ag, and PANI-Benz-Ag nanocomposite.

Sample	Size (d. nm)	PdI	Intercept
PANI	322.9	0.184	0.883
PANI-Benz	220.6	0.617	0.822
PANI-Ag	135.2	0.445	0.809
PANI-Benz-Ag	4.942	0.539	0.618

Table 2. The zeta potential values of PANI, PANI-Benz, PANI-Ag, PANI-Benz-Ag nanocomposite.

Sample	Zeta potential (mV)	Conductivity (μS/cm)
PANI	−2.39	5.1
PANI-Benz	−5.47	5.2
PANI-Ag	−7.28	8.52
PANI-Benz-Ag	−10.4	73.7

(−10.4 mV) and this might be due to a better electrostatic repulsion between particles which made it more stable compared to PANI, PANI-Benz, and PANI-Ag. This makes PANI-Benz-Ag more suitable for the detection of Endotoxin bacteria from adulterated and putrefied fruit juice.

The surface morphology of the PANI-Benz copolymer and PANI-Benz-Ag nanocomposite was analyzed by SEM [44, 45]. Figure 5(a) shows the presence of PANI and Benzimidazole polymers in the copolymer powder sample. The presence of Ag nanoparticles in the PAN-Benz-Ag nanocomposite is shown in figure 5(b). The SEM micrograph images show the structural morphology of PANI-Benzimidazole copolymer and Ag-doped PANI-Benz nanocomposite (figures 5 and 6). The silver nanoparticles are distributed with PANI-Benzimidazole copolymer during an *in situ* chemical oxidative polymerization reaction [46]. The Ag nanoparticles play a great role/interest in doping of conducting polymer such as PANI in the fabrication of sensor because its free conduction of electrons is released and incorporated into the polymer backbone due to the interaction process. Besides, Silver (Ag) particles have a high surface area and make its incorporated device have better chemical, mechanical and physical properties. Also, this makes Ag an important fluorescence nanomaterial with excellent potential for biosensor applications [47, 48].

The TEM images of Ag-doped at different loading (5–8 wt %) in PAN-Benz copolymer are shown in figures 6(a)–(f). The Ag nanoparticles at 5 wt % loading are shown in figures 6(a)–(c) and more agglomeration of Ag nanoparticles (6–8 wt %) incorporated PANI-Benz copolymers found in figures 6(d)–(f). The porous structure of PANI-Benz-Ag is shown in figure 6(c) and it can be suitable for the detection of Endotoxin *(E. coli bacteria)* in adulterated and putrefied juices [49].

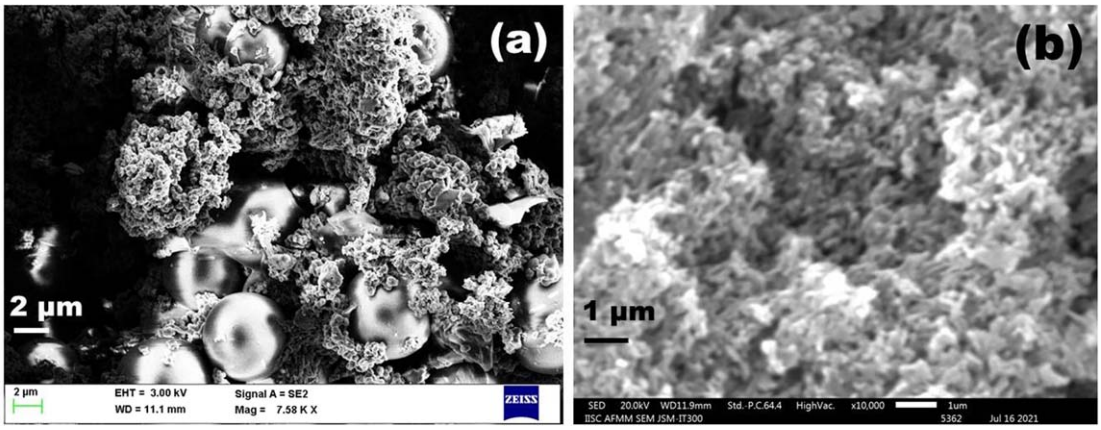

Figure 5. SEM Images of (a) PANI-Benz copolymer and (b) PANI-Benz-Ag nanocomposite.

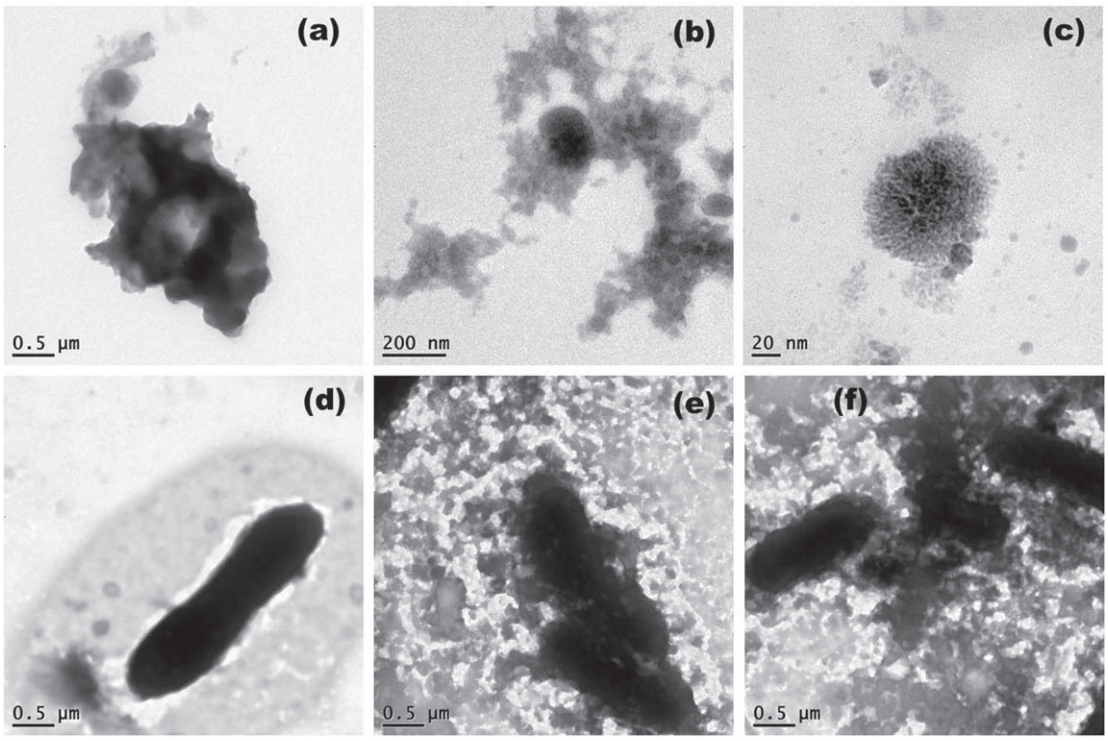

Figure 6. TEM Images of PANI-Benz-Ag nanocomposite at (a)–(c) 5 wt %, (d) 6 wt %, (e) 7 wt %, (f) 8 wt % loading of Ag nanoparticles.

The PANI-Ben-Ag nanocomposite was used to detect the Endotoxin by hitchhiking method (means of transportation for strangers like Endotoxin bacteria) which converts to an electrical signal. The dye 1, 9-dimethyl methylene zinc chloride blue (DMMB) was used with *E. coli* and PANI-Benz-Ag nanocomposite. The study involves the binding of Endotoxin with PANI-Benz-Ag nanocomposite using DMMB displacement assay [49]. The fabricated biochemical sensor (PANI-Benz-Ag nanocomposite) detects biochemical quantities such as endotoxin bacteria and converts the sensed endotoxin data into electronic data via an appropriate device called Confocal Imaging microscopy (Fluorescence). The fabricated biochemical sensor (PANI-Benz-Ag nanocomposite) could interact and converts biological information (concentration, activities of particles, partial pressure) of the interaction between it and the *E. coli* bacteria into a measurable signal. It transforms biochemical information ranging from the concentration of a specific sample component to total composition analysis into an analytically useful signal using its active sites via fluorescence. The active site of PANI-Benz-Ag nanocomposite (bioactive) comes into physical contact and interacts with the analyte/target molecules/ions in the sample (putrefied Mango Juice) in distinct ways. As a result, biochemical information is transported into a

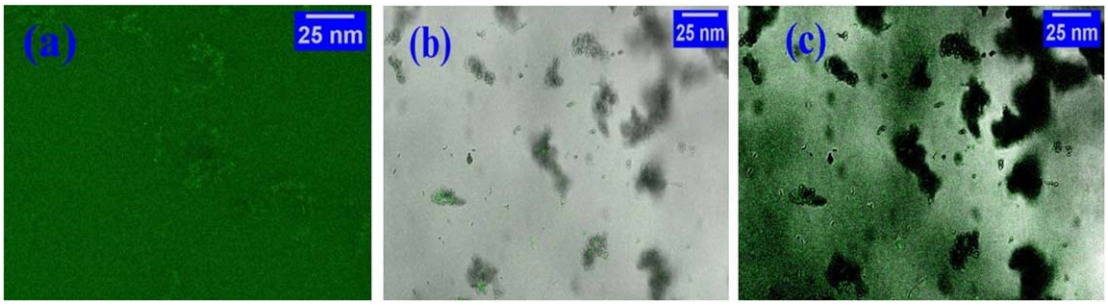

Figure 7. Confocal fluorescence microscopy analysis of endotoxin (a). DMMB, (b). DMMB + *E. coli* bacteria, and DMMB + *E. coli* bacteria + PANI-Benz-Ag nanocomposite.

form of energy that can be measured by its characterization device (Confocal Imaging microscopy/ fluorescence).

Since it is a single specific molecule sensor due to the presence of Benzimidazole, it recognizes the required endotoxin from the sample (Endotoxin putrefied Mango Juice) efficiently. As a result, the characterization device (Confocal Imaging microscopy/fluorescence) of the Ag-doped PANI-Benzimidazole nanocomposite was responsible for in-taking the biochemical information of the interaction between its active site and the Endotoxin. The biochemical information is converted into a measurable signal to obtain qualitative/or quantitative time and spatial resolved information about specific biochemical components such as fluorescence intensities/mean value of intensities, process areas, standard deviations, variance, etc These parameters change upon variations in the composition of biochemical species interacting with the sensor. Finally, this information is sent to a computer or mechanical component after transforming the energy into a useful analytical signal.

In the process, the excitation and emission of DMMB with and without *E. coli* bound with PANI-Benz-Ag nanocomposite were studied by quenching of DMMB fluorescence intensity (FI) using confocal fluorescence microscopy. As the Endotoxin bound to the PANI-Benz-Ag nanocomposite surface, it releases DMMB resulting in an increase in DMMB FI [49]. Figures 7(a)–(c) show the confocal fluorescence microscopic images of DMMB, DMMB+*E. coli* bacteria, and DMMB+*E. coli* bacteria + PANI-Benz-Ag nanocomposite respectively. The color intensity of images varies from the figure. (a) and (b) to (c) due to the binding effect of *E. coli* bacteria on DMMB +PANI-Benz-Ag nanocomposite. The increase in color intensity of the image in the figure. (c) confirms the detection of *E. coli* bacteria using PANI-Benz-Ag nanocomposite [49].

The binding of Endotoxin *(E. coli)* bacteria on PANI-Benz-Ag nanocomposite surface and the increase in FI of DMMB could be explained by plotting the average intensity (*y*-axis) versus average process area (*y*-axis) from the region of interest (ROI) of confocal microscopic images (figure 8).

In the absence of Endotoxin bacteria, the FI of DMMB exhibited a higher average mean value (140 a.u.). However, the addition of Endotoxin bacteria *(E. coli)* to DMMB sharply decreased the FI which indicates the fast binding and rapid saturation of DMMB with Endotoxin by quenching mechanisms. The mixture of DMMB+*E. coli* was added to the PANI-Benz-Ag nanocomposite. The particles of nanocomposite competitively bound to Endotoxin *(E. coli)* bacteria which displaced the binding of *E. coli* with DMMB as observed from the FI of Confocal Fluorescence microscopy images. As a result, the FI of DMMB was increased from its quenched state at equilibrium with Endotoxin which indicates the increase in binding of *E. coli* to PANI-Benz-Ag nanocomposite particles. This proves that PANI-Benz-Ag nanocomposite can be used as a sensor for the detection of Endotoxin *E. coli* bacteria from adulterated foods stuff such as putrefied mango juice, etc.

4. Conclusion

An effective and new Ag-doped-PANI-Benzimidazole copolymer nanocomposite material, which can bring recent advances and a paradigm shift towards the use of electrochemical biosensors to detect Endotoxin *(E. coli)* bacteria. The Zetasizer was used to determine the size of the PANI-Benz-Ag nanocomposite particles (4.942 nm). The FTIR data showed the quinoid units along the polymer chain being affected, such that strong interactions between Ag nanoparticles and quinoidal sites of PANI were presumed. The XRD analysis confirmed the amorphous and crystalline nature of PANI, PANI-Benz copolymer, and PANI-Benz-Ag nanocomposite. The morphological study confirmed the formation and distribution of Ag nanoparticles in the PAN-Benz copolymer surface. The characteristic absorption peaks of the fabricated material analysis (UV-Visible spectrum) were very appropriate and depictable. Confocal Imaging microscopy using 1, 9-dimethyl methylene zinc blue (DMMB) fluorescence displacement-based assay method showed that PANI-Benz-Ag (bioactive)

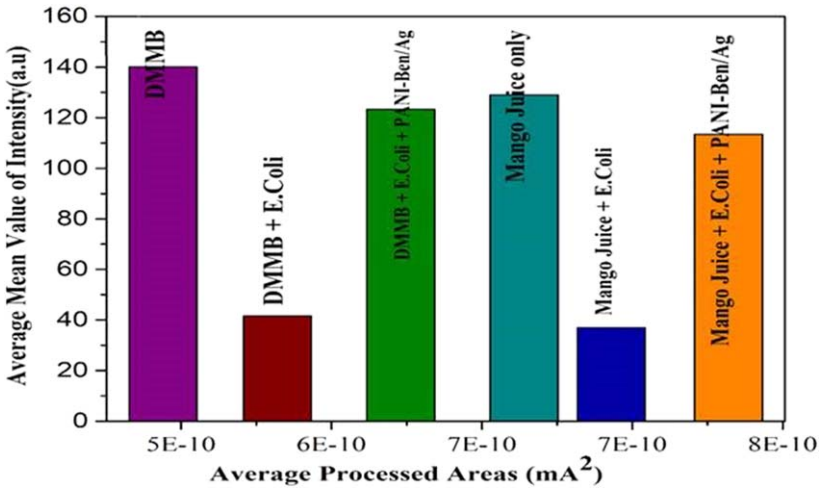

Figure 8. Histogram of fluorescence intensity versus Average processed area for DMMB, DMMB+*E. coli*, DMMB+*E. coli*+PANI-Benz-Ag, and Mango juice+*E. coli*+PANI-Benz-Ag.

nanocomposite can be used as a good electrochemical biosensor for the detection of Endotoxin *(E. coli)* bacteria from putrefied Mango juice.

Acknowledgments

The authors thank Jimma University, Ethiopia, and the Indian Institute of Science, India for providing financial support and laboratory facilities to carry out the research work.

Data availability statement

All data that support the findings of this study are included within the article (and any supplementary files).

Conflict of interest

The authors declare that there is no conflict of interest.

ORCID iDs

Delele Worku Ayele https://orcid.org/0000-0002-9319-6334
Dhakshnamoorthy Mani https://orcid.org/0000-0002-1065-8346

References

[1] Sharma K and Paradkar M 2010 Erratum to the melamine adulteration scandal *Food Security.* **2** 109
[2] Sharma K and Paradakar M 2010 The melamine adulteration scandal *Food Security.* **2** 97–107
[3] Adamik B *et al* 2015 Endotoxin elimination in patients with septic shock: an observation study *Archivum immunological et therapies experimental.* **63** 475–83
[4] Barrett A C *et al* 2016 Utilizing geographic information systems to identify clusters of severe sepsis patients presenting in the out-of-hospital environment *Prehospital Emergency Care.* **20** 200–5
[5] Su W and Ding X 2015 Methods of endotoxin detection *SLAS Technology.* **20** 354–64
[6] Vrieze A *et al* 2013 Fecal transplant: a safe and sustainable clinical therapy for restoring intestinal microbial balance in human disease? *Best Practice & Research Clinical Gastroenterology.* **27** 127–37
[7] Seok J *et al* 2013 Genomic responses in mouse models poorly mimic human inflammatory diseases *Proc. Natl Acad. Sci.* **110** 3507–12
[8] Brade H 2020 *Endotoxin in Health and Disease.* (Boca Raton, FL: CRC Press)
[9] Tejada D *et al* 2015 Lipoproteins/peptides are sepsis-inducing toxins from bacteria that can be neutralized by synthetic anti-endotoxin peptides. *Sci. Rep.* **5** 1–15
[10] Boonen B *et al* 2018 TRP channels as sensors of bacterial endotoxins *Toxins.* **10** 326
[11] Meseguer V *et al* 2014 TRPA1 channels mediate acute neurogenic inflammation and pain produced by bacterial endotoxins *Nat. Commun.* **5** 3125
[12] Puligundla P and Lim S 2022 Biocontrol approaches against Escherichia coli O157: H7 in foods *Foods.* **11** 756

[13] Mengistu D A *et al* 2022 Bacteriological quality of locally prepared fresh fruit juice sold in juice houses of eastern Ethiopia *Environmental Health Insights.* **16** 11786302211072949
[14] Mihiretie H and Desta K 2015 Microbiological criteria and quality of fruits and fruit juices in Ethiopia and international experience *J Med Microbiol Diagn.* **4** 207
[15] Bello O O, Temitope K B and Muibat O F 2014 Microbiological quality of some locally-produced fruit juices in Ogun state, southwestern Nigeria *E3 J Microbiol Res.* 2, 001–008
[16] Bulti K F and Melkam D L 2018 Microbiological quality of fruit juices sold in cafes and restaurants of Shewarobit town, Amhara, Ethiopia. African *Journal of Microbiology Research.* **12** 623–8
[17] Maffei D F *et al* 2016 Microbiology of organic and conventionally grown fresh produce *Brazilian Journal of Microbiology* **47** 99–105
[18] Yang S-C *et al* 2017 Current pathogenic Escherichia coli foodborne outbreak cases and therapy development *Arch. Microbiol.* **199** 811–25
[19] Salomão B D C M 2018 Pathogens and spoilage microorganisms in fruit juice: an overview. *Fruit juices.* 291–308
[20] Mohammadpour H *et al* 2018 The prevalence of Campylobacter spp. in vegetables, fruits, and fresh produce: a systematic review and meta-analysis *Gut pathogens.* **10** 1–12
[21] Ehuwa O, Jaiswal A K and Jaiswal S 2021 Salmonella, food safety and food handling practices *Foods.* **10** 907
[22] Callejón R M *et al* 2015 Reported foodborne outbreaks due to fresh produce in the United States and European Union: trends and causes *Foodborne Pathogens and Disease.* **12** 32–8
[23] Augustin J-C *et al* 2020 Contribution of Foods and Poor Food-Handling Practices to the Burden of Foodborne Infectious Diseases in France. *Foods* **9** 1644
[24] Bhaskar S 2017 *Foodborne Diseases—Disease Burden, in FOOD Safety in the 21st Century.* (Amsterdam: Elsevier) 1–10
[25] Li H *et al* 2021 Characteristics of settings and etiologic agents of foodborne disease outbreaks–China, 2020 *China CDC Weekly.* **3** 889
[26] Rietschel E T *et al* 1993 The chemical structure of bacterial endotoxin in relation to bioactivity *Immunobiology.* **187** 169–90
[27] Elkhateeb M A, Elkhatib W and Aboulwafa M 2019 An expert review on current approaches for endotoxin detection in various biological products *Archives of Pharmaceutical Sciences Ain Shams University.* **3** 142–53
[28] Roslansky P F and Novitsky T J 1991 Sensitivity of Limulus amebocyte lysate (LAL) to LAL-reactive glucans *J. Clin. Microbiol.* **29** 2477–83
[29] Dullah E C and Ongkudon C M 2017 Current trends in endotoxin detection and analysis of endotoxin–protein interactions *Crit. Rev. Biotechnol.* **37** 251–61
[30] Cao Y, Zhang Y and Qiu F 2021 Low endotoxin recovery and its impact on endotoxin detection *Biopolymers.* **112** e23470
[31] Fung F M *et al* 2017 Extraction, separation and characterization of endotoxins in water samples using solid phase extraction and capillary electrophoresis-laser induced fluorescence *Sci. Rep.* **7** 1–10
[32] Wachtel R E and Tsuji K 1977 Comparison of Limulus amebocyte lysates and correlation with the United States pharmacopeial pyrogen test *Appl. Environ. Microbiol.* **33** 1265–9
[33] Ding J L and Ho B 2001 A new era in pyrogen testing *Trends Biotechnol.* **19** 277–81
[34] Abu-Thabit N Y 2016 Chemical oxidative polymerization of polyaniline: a practical approach for preparation of smart conductive textiles *J. Chem. Educ.* **93** 1606–11
[35] Kandulna R and Choudhary R 2017 Robust electron transport properties of PANI/PPY/ZnO polymeric nanocomposites for OLED applications *Optik* **144** 40–8
[36] Tamboli M S *et al* 2012 Nanowires of silver–polyaniline nanocomposite synthesized via in situ polymerization and its novel functionality as an antibacterial agent *Colloids Surf.*, B **92** 35–41
[37] Ahad I Z M *et al* 2018 Polyaniline (PAni) optical sensor in chloroform detection *Sensors Actuators* B **261** 97–105
[38] Wasu M and Raut A 2014 Synthesis and characterization of polyaniline based conducting polymers *Journal of Chemistry.* **4** 90–7
[39] Phatake V V and Bhanage B M 2019 Cu@ UgC 3 N 4 catalyzed cyclization of o-phenylenediamines for the synthesis of benzimidazoles by using CO 2 and dimethylamine borane as a hydrogen source *Catal. Lett.* **149** 347–59
[40] Sunny V *et al* 2006 Evidence for intergranular tunneling in polyaniline passivated α-Fe nanoparticles *Nanotechnology* **17** 4765
[41] Zengin H *et al* 2019 Preparation and characterization of conductive polyaniline/silver nanocomposite films and their antimicrobial studies *Polymer Engineering & Science.* **59** E182–94
[42] Buzea C, Pacheco I I and Robbie K 2007 Nanomaterials and nanoparticles: sources and toxicity *Biointerphases.* **2** MR17–71
[43] Ramaye Y *et al* 2021 Development and validation of optical methods for zeta potential determination of silica and polystyrene particles in aqueous suspensions *Materials.* **14** 290
[44] Imani A and Farzi G 2015 Facile route for multi-walled carbon nanotube coating with polyaniline: tubular morphology nanocomposites for supercapacitor applications *J. Mater. Sci., Mater. Electron.* **26** 7438–44
[45] Matindoust S *et al* 2017 Ammonia gas sensor based on flexible polyaniline films for rapid detection of spoilage in protein-rich foods *J. Mater. Sci., Mater. Electron.* **28** 7760–8
[46] Heffner G *et al* 1993 The effect of molecular weight and crystallinity on the conductivity of a conducting polymer *Polymer* **34** 3155–9
[47] Deng C *et al* 2022 An emerging fluorescent carbon nanobead label probe for lateral flow assays and highly sensitive screening of foodborne toxins and pathogenic bacteria *Anal. Chem.* **94** 11514–20
[48] Wang B *et al* 2021 Carbon dots as a new class of nanomedicines: opportunities and challenges *Coord. Chem. Rev.* **442** 214010
[49] Donnell M L *et al* 2016 Endotoxin hitchhiking on polymer nanoparticles *Nanotechnology* **27** 285601